https://doi.org/10.1016/j.ces.2021.116961

Stochastic Optimization-based Approach for Simultaneous Process Design and HEN Synthesis of Tightly-coupled RO-ORC-HI Systems Under Seasonal Uncertainty

Zhichao Chen[a], Zhibin Lu[b], Bingjian Zhang[b], Qinglin Chen[b], Chang He*[b], Haoshui Yu*[c], Jingzheng Ren[d]

[a] School of Chemical Engineering and Technology, Sun Yat-sen University, Zhuhai, 519082, China

[b] School of Material Science and Engineering, The Key Laboratory of Low-carbon Chemistry & Energy Conservation of Guangdong Province, Sun Yat-sen University, Guangzhou, 510006, China

[c] MIT Energy Initiative, Massachusetts Institute of Technology, 77 Massachusetts Avenue, Cambridge, MA, 02139, USA

[d] Department of Industrial and Systems Engineering, The Hong Kong Polytechnic University, Hong Kong Special Administrative Region, China

Submitted to ***Chemical Engineering Science***

*Corresponding authors: Prof. Chang He, E-mail: hechang6@mail.sysu.edu.cn;

*Corresponding authors: Dr. Haoshui Yu, E-mail: yuhaoshui1@126.com.

Abstract

The use of waste heat powered wastewater desalination by coupling an organic Rankine cycle (ORC) with reverse osmosis (RO) has been recognized as a promising solution to desalination. Herein, a tightly-coupled system that allows for optimally customizing the RO-ORC to a background process via heat integration (HI) is developed to minimize the expected desalination cost, while accounting for the seasonal wastewater variability. Moreover, the developed RO-ORC-HI system can improve the membrane permeability by preheating the feed wastewater. To achieving these goals, a stochastic optimization-based solution strategy is proposed by sequentially considering (1) a Pinch-based Duran-Grossman model embedded with uncertainty realization for performing optimal HI during process optimization; (2) a flexible multi-scenario heat exchanger net (HEN) synthesis model that minimizes the total annualized cost of HEN based on a customized stage-wise superstructure. Finally, the behaviors of the proposed system and solution strategy are illustrated through its comparison with a deterministic solution.

Keywords

Waste heat powered desalination, Rankine cycle, reverse osmosis, seasonal uncertainty, stochastic optimization, Duran-Grossman model, flexible HEN synthesis

Nomenclature

Indices			
id	ideal	φ	A big constant
in	inlet		
k	stage	Sets	
out	outlet	C	cold streams
p	Pinch candidate	C'	extended cold streams
R	residual	EQP	ORC equipment
c	critical	GSP	gas state points
cu	cold utility	H	hot streams
cw	cooling water	LSP	liquid state points
ele	electricity	PC	Pinch candidates
hu	hot utility	S	scenarios
i	process hot stream/ORC equipment/ RO stage	SP	State points
j	process cold stream	STR	process streams

s	scenario		
sp	state point of ORC	Binary Variable	
sub	subcooled	y	Existence of the heat exchanger
sup	superheating		
tp	two phase	Continuous Variable	
SW	Saline wastewater	CC	Capital cost
		CPF	Concentration polarization factor
Parameters		FCp	Heat capacity flowrate
A	Temperature related dimensionless coefficients/ membrane permeability	HD	Heat deficit
AF	Annualized factor	dt	Temperature difference of the exchanger
B	Pressure related dimensionless coefficient	m	Mass flowrate
CNup	Maximum allowed conductance	OC	Operating cost
Cp	Heat capacity	P	Pressure
Ea	Activated energy	Q	Heat load
FF	Fouling factor	q	Heat load of the heat exchanger in the superstructure
HRAT	Heat recovery approach temperature	Qp	Total flow rate of permeate
HW	Hot water	QSIA	Heat load of cold streams above the Pinch candidates

J	Permeate flux across a membrane element	QSOA	Heat load of hot streams above the Pinch candidates
NOK	Number of stages in superstructure	sldt	Slack variable for temperature approach violations
NOS	Number of scenarios	T	Temperature
OT	Operating time	TAC	Total annualized cost
PGP	Power generation profit	TCF	Temperature correction factor
prob	Probability of occurrence of a specific feeding scenario	W	Work
R	Ideal gas constant	Z	Compressibility factor
u	Constant	$\mathbf{Z}$	Sum of slack variables
w	Constant	Π	Osmotic pressure
ε	A small constant	$\overline{\Delta\Pi}$	Actual osmotic pressure difference

1. Introduction

Both waste heat and wastewater are inevitable by-products of the process industries such as petrochemical, thermo-power, and metallurgy plants. It is reported that more than 50% of the energy that is used in the world is wasted as low-grade heat (Mahmoudi et al., 2018). Most of the waste heat is ultimately discharged into the ambient due to a lack of receiving users, which in turn causes enormous energy losses and additional environmental impacts. Meanwhile, the inorganic salt ions (i.e., Na^{+}, Ca^{2+}, Cl^{-}, and SO_4^{2-}) are easy to accumulate during each unit operation but hard to dispose of, resulting in a large amount of high-salinity wastewater at a concentration of 3000~8000 ppm (Zhu et al., 2017). Due to the growing concerns over brine disposal, most countries and regions have forced the process industries to operate with more rigorous discharge specifications or even zero liquid discharge. Treating such high-salinity wastewater for reuse or discharge would consume a massive amount of energy, which is responsible for more than half of the desalination cost (Pan et al., 2020). This indicates that waste heat and wastewater are inextricably and reciprocally dependent from the viewpoint of water-energy nexus, thus entailing a need to integrally address the industrial waste heat recovery and high-salinity wastewater treatment.

In the past decade, considerable efforts have been made to minimize the energy cost for high-salinity wastewater treatment by developing various integrated waste heat-driven thermal desalination technologies such as multi-stage flash (Janajreh et al., 2013), multi-effect distillation (Mohammed et al., 2021), thermal vapor compression (Cao et al., 2018), and other hybrid systems (Goh et al., 2021). Recently, membrane-

based reverse osmosis (RO) desalination has played a dominant role in new installations in the process industry due to its advantages over thermal desalination in modularized design and installation, lower capital cost, and higher energy efficiency. Despite these advantages, the energy intensity (about 0.8~2.5 kWh/m^3) remains a major drawback for the application of RO desalination. This is caused by the fact that RO desalination only relies on electricity or mechanical energy, instead of thermal energy, to drive the pumps and other electrical components, which takes up to about 50~80% of an RO facility's operational and maintenance costs especially as operated at high water recoveries. (Abdelhady et al., 2015)

The organic Rankine cycle (ORC) is a mature technology to recover low-grade thermal heat for power generation, which enables the development of waste heat-driven wastewater desalination by coupling RO and ORC. In principle, the maximum amount of energy recovered by ORC depends on the heat transfer behavior between working fluid and waste heat source. The previous studies mainly focused on improving the techno-economic behaviors of the coupled system by (1) selecting the most appropriate type and composition of the working fluids (Zhang et al., 2021), and (2) integrally designing of processes and working fluids for ORCs (Schilling et al., 2021). Besides, note that there are generally multiple waste heat sources in practice that need to be recovered from the industrial background process. For this reason, the techno-economic parameters of ORC and its heat integration (HI) with the background process should be optimized simultaneously to take better advantage of ORCs. This leads to a challenging issue for HI since the flow rates and temperatures of some participated streams are

variable.

In order to obtain a feasible solution, Duran and Grossmann (1986) pioneered a sequential method that synthesized the heat exchanger network (HEN) and utility system while considering all the possible integration options between process and utility system. Desai and Bandyopadhyay (2009) proposed a Pinch-based heuristic method for appropriate integration and synthesis of an ORC as a cogeneration process with a background process. Chen et al. (2014) proposed a two-step method in which the HEN is optimized before the integration with the heat recovery cycle. Yu et al. (2017) adopted the Duran-Grossmann model (1986) for integrating an ORC into a background process, which optimally considered the modifications of the ORC to increase the thermal efficiency and heat recovered by the working fluid. Martelli et al. (2017) proposed an MINLP model and two-stage algorithm to tackle the simultaneous synthesis of completely integrated utility systems and HENs. Xuan et al. (2020) proposed a two-level optimization strategy for the simultaneous optimization of ORC and HI involving the area estimation of heat exchangers with variable temperatures and flowrates based on vertical heat transfer of Pinch technology. In Elsido et al. (2021a), they proposed a new sequential algorithm based on the idea of optimizing the independent mass flow rates of the Rankine cycle superstructure with a derivative-free algorithm. In all, these sequential methods do not allow to rigorously optimize the trade-off between capital cost, operating cost, and energy efficiency due to their sequential decomposition. Besides, utility systems are selected and sized in the first step by solving a MILP problem which only requires a linear objective function (Elsido et al., 2019).

It is worth noting that most of the previous studies focused on the simultaneous process optimization and HI of the stand-alone ORC integrated with a background process without consideration of uncertainty. As the RO desalination is further coupled with an ORC, however, the variability of the industrial wastewater stream has to be addressed since it is considerably more variable in salinity, flow rate, and temperature in different seasons. For instance, in coal-chemical plants, the salinity profile of the wastewater entering the disposal facility generally shows an evident upward trend as both flow rate and inlet temperature are reduced in cold seasons. Besides, the experimental studies highlighted that the permeability of the membranes was more affected by the feed temperature rather than the feed pressure and concentration. (Shaaban and Yahya, et al., 2017) The permeate flux can increase by up to 60% as the feed temperature increases from 20 ºC to 40 ºC, which theoretically leads to much lower specific energy consumption. Nevertheless, the energy benefit of running a RO plant over a range of temperatures is significant only as the temperature variation covers a limited range due to the complex correlation among temperature, flow rate, and salinity of the feed wastewater (Huang et al., 2019). Ignorance of the variation and correlation of these parameters makes it is hard to maintain a feasible and steady-state operation, which leads to an impractical techno-economic behavior of the coupled system.

From the abovementioned background, it is found that dealing with the uncertainty on feed wastewater has become one of the practical issues in optimally customizing an RO-ORC into an industrial background process. In the last decades, various solution methods for flexible HEN synthesis have been developed to account for the different

uncertainties (Kang and Liu, 2019). These methods can be classified into four main categories that include sensitivity analysis (Hafizan et al., 2020), resilience and flexibility analysis (Zhang, 2011), and multi-scenario synthesis (Elsido et al., 2021b). Although the previous methods made it possible to perform flexible HEN synthesis with consideration of variable temperatures and flow rates, the detailed process design has been ignored due to their computational difficulty when integrated with HEN. For the considering coupled system, note that the wastewater variability not only affects the HEN topology, but also has a profound impact on both waste heat recovery and membrane performance. To the best of our knowledge, there is existing literature on the deep integration of ORC, RO, and HI under uncertainty for integrally addressing the practical issue of waste heat recovery and wastewater treatment under uncertainty. Moreover, existing literature do not report any approach to improve the performance of membrane simultaneously in the optimal design and synthesis of the coupled system.

In this study, a new industrial waste heat-driven RO-ORC-HI system is developed for producing qualified permeate under changing feed wastewater conditions. It not only allows for the efficient integration of the RO-ORC into a background process with HI, but also the remarkable improvement in membrane permeability by flexibly adjusting the preheating temperature of the feed wastewater. To perform simultaneous stochastic process optimization and flexible HEN synthesis, the problem is first decomposed into five sub-problems, which are solved sequentially by using a two-step solution strategy. In particular, a finite number of correlated scenarios that accommodate the diverse nature of wastewater (salinity, flow rate, and temperature) is

generated via the Monte Carlo sampling technique. It is then embedded in a Pinch-based Duran-Grossman model for minimizing the total annualized cost of the coupled system without considering the detailed HEN topology. Based on a customized stage-wise superstructure, the multi-scenario HEN of the coupled system is synthesized by sequential flexibility test and isothermal mixing assumption removal. Finally, an illustrative example based on a styrene plant is used to verify the effectiveness of the proposed strategy.

2. Problem Statement

The coupled system as illustrated in Fig. 1 can be divided into three interactive subsystems namely HI, ORC, and RO subsystems. The problem addressed in the study is stated as follows. Within the background process, given are a set of hot and cold streams (H and C) with known heat capacity flow rates, and each process stream has to be cooled or heated from its supply temperature to the target value. In addition, a set of available hot and cold utilities (HU and CU) is specified. To present a highly integrated RO-ORC-HI system, both the hot water (HW, in the ORC subsystem) and the feed wastewater (SW, in the RO subsystem) can exchange heat with process streams in the background process. Specifically, they are regarded as cold streams to recover the waste heat from the background process. The extended sets of the cold streams and all process streams are defined as $C' = C \cup \{SW, HW\}$ and $STR = H \cup C'$, respectively. The power generated by ORC is mainly used for driving the pumps and other electrical components of the RO subsystem. If the power generation is enough, the surplus power can be directly sold at market price to reduce the desalination costs. Otherwise, on-grid

electricity can make up for the shortage of supply.

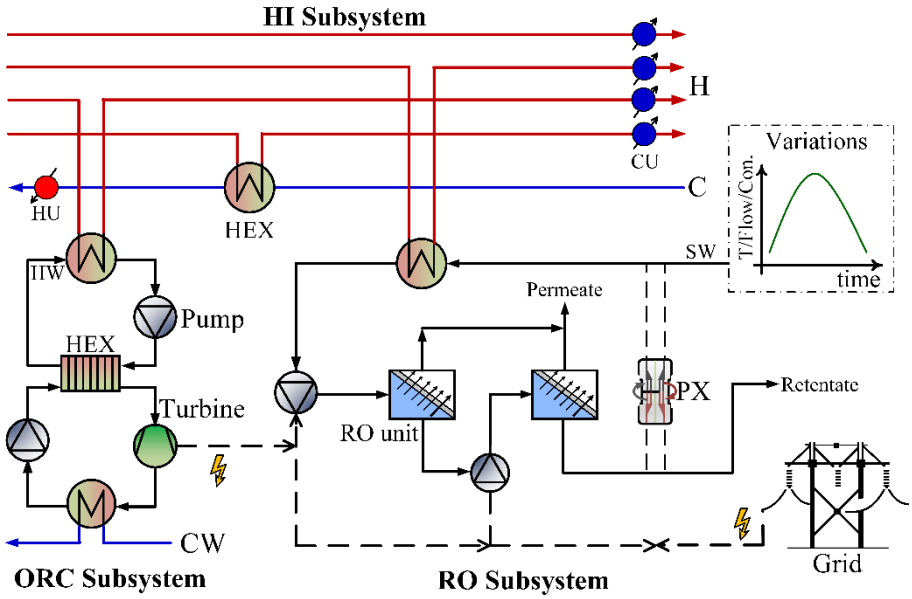

Fig. 1. The schematic diagram of the coupled RO-ORC-HI system

In Fig. 1, the saline wastewater entering the RO desalination is considerably more variable in salinity, flow rate, and temperature in different seasons based on a long-term recording. Additionally, note that these uncertain parameters normally have symmetric correlations, i.e., it is observed that the flow rate profile of wastewater generally shows an evident increase as the ambient temperature increases from a cold season to a warm one; whereas in turn, the increased flow rate lowers the salinity of wastewater. The variability of these correlated parameters not only would decrease the techno-economic benefits of process integration among three subsystems, but also has an underlying impact on HI performance and HEN topology. These uncertain parameters, together with the variable hot water in the ORC subsystem, making it hard for conventional combined HEN synthesis and process optimization methods to handle such problems. From the abovementioned statements, the research challenges of the developed RO-ORC-HI system mainly include how to properly account for seasonal variability related

to the feed wastewater, how to develop optimal process designs based on stochastic optimization, and how to synthesize the flexible HEN during stochastic optimization with unknown/uncertain variables.

3. Outline of the Solution Strategy

To address the research challenges related to the developed RO-ORC-HI system, the problem is decomposed into five sub-problems and solved sequentially by a two-step solution strategy, as illustrated in Fig. 2. In step I, it seeks to perform the stochastic optimization of the developed process flow sheet while handling the problem of optimal HI. First, Pinch-based Duran-Grossman model (Duran and Grossmann, 1986) coupled with ORC thermodynamic model and RO desalination model is adopted to perform simultaneous HI and process optimization. A deterministic non-linear programming (NLP) model (**P1**) that only accounts for the nominal conditions is formulated for the coupled system. Thereafter, a stochastic multi-scenario NLP model (**P2**) is developed by modifying (**P1**) to fully account for the diverse nature of the wastewater variability. In (**P2**), we employ a correlated scenarios generation approach that includes uncertainty characterization and Monte Carlo sampling to process input data and generate a proper size of distinct correlated scenarios (periods), as detailed in Section 4.1.4. Based on the solution of (**P2**), the maximum waste heat recovery and the minimum consumption of hot and cold utilities without considering detailed HEN are obtained. Also, the corresponding optimal flow rate, inlet and outlet temperatures of hot water, as well as the outlet temperature of saline wastewater in each scenario are resolved.

In step II, to further obtain the detailed HEN, the generated scenarios should be

divided into two groups, namely initial and testing scenarios. The initial scenarios are incorporated into a multi-scenario HEN synthesis model (**P3**) to derive the HEN topology by minimizing the total annualized cost of the HEN (TAC_{HEN}). The obtained structure of the HEN and the maximum allowed conductance (CNup) of each heat exchanger are further used as input parameters for performing a flexibility analysis in (**P4**). Meanwhile, the testing scenarios are sequentially passed to (**P4**) to validate the flexibility of the network. If the result of a flexibility test does not satisfy the target, the corresponding testing scenario will be identified as the "critical scenario". The critical scenarios together with initial scenarios are all passed to model (**P3**) to re-synthesize the multi-scenario HEN. This iteration process continues to execute until all testing scenarios satisfy the flexibility target. For a specific HEN that has passed the flexibility test, the isothermal mixing assumption should be removed from the HEN. For this purpose, an NLP improvement model (**P5**) is finally developed by fixing the binary variables.

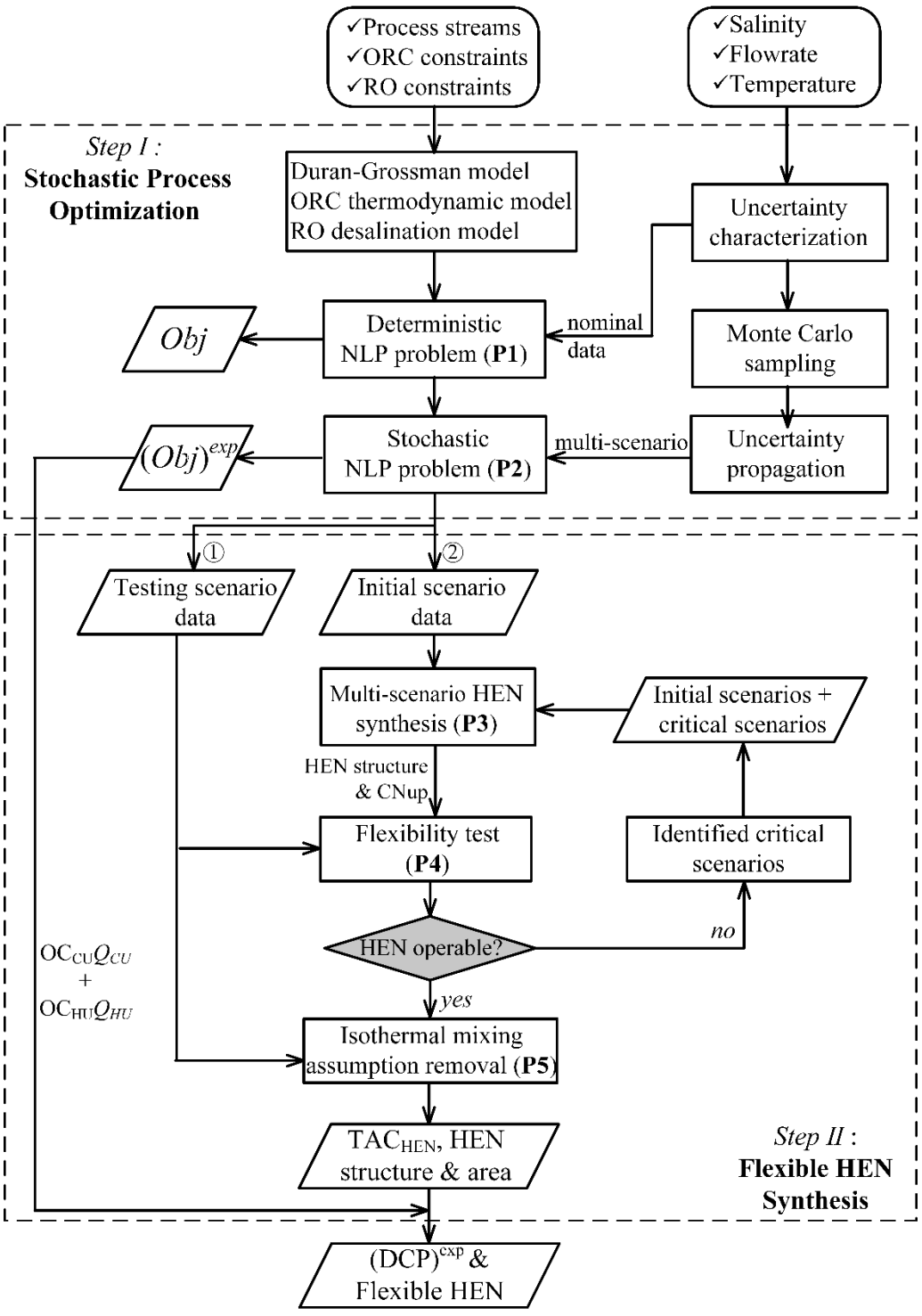

Fig. 2. Outline of the solution strategy

Through sequentially solving (**P2**)~(**P5**), the minimum expected desalination cost of the coupled system with flexible HEN is obtained. The final HEN design consists of the optimal placements of heat exchangers, heaters, coolers, as well as the minimum

sizes of heat-transfer units which ensure feasible operations within the specified ranges of uncertainty.

4. Model Description and Formulation

4.1. RO-ORC-HI system

In this section, the process synthesis and formulation of the RO-ORC-HI system are detailed for both deterministic and stochastic methods. To reduce the computational burden, the following assumptions are adopted: (a) constant physical properties; (b) regenerator and turbine bleeding are not included in ORC modelling; (c) an isothermal RO membrane; (d) influence of temperature variation on salt passage across the membrane channel is ignored (Wang et al., 2018); (e) feed wastewater only contains monovalent salt (NaCl) and is supplied at the ambient temperature (Li, 2015); (f) counter-current heat exchanger without pressure drop and fluid dynamics; (g) only utility duties and bypasses can be adjusted during operation of the heat exchanger.

4.1.1 Duran-Grossmann model

The HI subsystem collects all process streams from the background process, along with the hot water and saline wastewater streams from the ORC and RO subsystems to perform HI. In this coupled system, the heat loads of hot water and wastewater streams, as well as the heat capacity flow rate of ORC are unknown or uncertain. For addressing this issue, Duran-Grossmann model is adopted for automatically implementing HI during process optimization. This model is based on the Pinch method, but fixed temperature intervals are not required to determine the energy target. Instead, the inlet

temperatures of all streams are considered as Pinch candidates defined as $PC = \{T_i^{in} | \ i \in STR\}$. The inlet temperatures of hot streams are considered as Pinch candidates. As for cold streams, the Pinch candidates are the sum of their inlet temperatures and the heat recovery approach temperature (HRAT), which is set as 10 ºC (Tajik Mansouri et al., 2019) in this study.

$$T_i^p = T_i^{in}, \ i \in H, p \in PC \tag{1}$$

$$T_j^p = T_j^{in} + HRAT, \ j \in C', p \in PC \tag{2}$$

In this way, the heat loads of all hot and cold streams (*QSOA* and *QSIA*) above the corresponding Pinch candidates can be calculated by Eqs. (3) and (4), respectively.

$$QSOA(x)^p = \sum_{i \in H} FCp_i \left[\max\{0, T_i^{in} - T^p\} - \max\{0, T_i^{out} - T^p\} \right], \ p \in PC \tag{3}$$

$$QSIA(x)^p = \sum_{j \in C'} \begin{bmatrix} \max\{0, T_j^{out} - (T^p - HRAT)\} \\ -\max\{0, T_j^{in} - (T^p - HRAT)\} \end{bmatrix}, \ p \in PC \tag{4}$$

The heat deficit above each Pinch candidate is derived by Eq. (5). Then, the Pinch point is considered as the Pinch candidate with maximum heat deficit, and the corresponding hot utility consumption can be determined by Eq. (6).

$$HD^p(x) = QSIA(x)^p - QSOA(x)^p, \ p \in PC \tag{5}$$

$$Q_{hu}(x) \geq HD^p(x), \ p \in PC \tag{6}$$

Once the hot utility is determined, the cold utility can be derived from a heat balance as shown in Eq. (7).

$$Q_{cu} = Q_{hu} + \sum_{i \in H} FCp_i (T_i^{in} - T_i^{out}) - \sum_{j \in C'} FCp_j (T_j^{out} - T_j^{in}) \tag{7}$$

It should be pointed out that most of the NLP solvers require a continuous first-order differential. Therein, a smooth function is imported to approximate the max operators in Eqs. (3) and (4), as given by

$$\max\{0,\xi\} \approx \frac{1}{2}\left[\xi + \sqrt{\xi^2 + \varepsilon}\right] \tag{8}$$

where ξ is the scalar argument and ε is a small constant between 10^{-3} and 10^{-6}.

4.1.2 ORC thermodynamic model

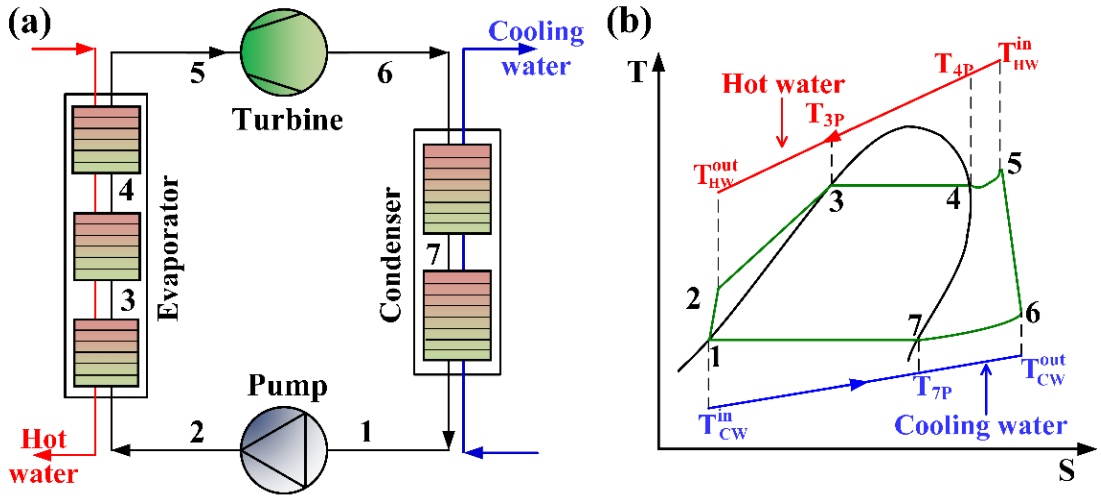

Fig. 3. (a)The ORC flowsheet and (b) T-S diagrams of ORC

Accurate thermodynamic properties calculation is computationally challenging in both process simulation and optimization. To obtain a reliable solution of the coupled system, a rigorous thermodynamic model of ORC must be constructed. This is essential to predict the true physical conditions of organic working fluid and intermedium as mathematically integrating an ORC into the background process. In this study, R600a (isobutane) is chosen as the working fluid of ORC. To improve the safety of the operation, hot water is used as an intermedium to transfer heat from the heat source to the working fluid. Fig. 3(a) shows the schematic flowsheet of the ORC subsystem. Here, seven different states for modelling the ORC are chosen and mapped into the T-S diagram as shown in Fig. 3(b). Thus, a state point set $SP=\{sp|1, 2, 3, 4, 5, 6, 7\}$ that refers to the thermodynamic state at different points is defined to facilitate the model

formulation. Furthermore, to avoid the coincidence issue of state points 4 and 5 in the non-superheating thermodynamic cycle, the set *SP* can be divided into two subsets, namely liquid state points *LSP*={*lsp*|1, 2, 3} and gas state points *GSP*={*gsp*|4, 5, 6, 7}. For each of the phase conditions at the state points, Peng-Robinson equation of state is used for thermodynamic properties calculation due to its applicability to wide ranges of temperature and pressure. The form of this equation for pure components is given by:

$$Z_{sp}^3-(1+B-uB)Z_{sp}^2+(A+wB^2-uB-uB^2)Z_{sp}-AB-wB^2-wB^3=0,\ sp\in SP \quad (9)$$

where Z is the compressibility factor; A and B are temperature- and pressure-related dimensionless coefficients; u and w are the constants that rely on the actual equations of state, herein u=2 and w=–1 (Yu et al., 2018). The detailed information for the Peng-Robinson equation is provided in Section 1 of Supplementary Information (SI).

Once the thermodynamic properties calculation is completed, the energy balance and cost estimation in ORC operation can be determined sequentially, as detailed in Eqs. (S9)~(S33) in SI. The total annualized cost of this subsystem (TAC_{ORC}) as well as the power generation profit (PGP) are given by

$$TAC_{ORC}=OC_{cw}\times m_{cw}\times Cp+AF\times\sum_{i\in EQP}CC_i \quad (10)$$

$$PGP=OT\times Pr_{ele}\times W_{ORC} \quad (11)$$

where OC_{cw}, m_{cw}, and Cp represent the operating cost, mass flow rate, and heat capacity of cooling water used in the subsystem, respectively; AF, OT, and Pr_{ele} represent the annualized factor, operating time, and electricity price, respectively; CC_i represents the capital cost of equipment i in equipment set *EQP*, as given by Eqs. (S25)~(S33) in SI.

4.1.3 RO desalination model

As shown in Fig. 4, a dual-stage, once-through RO desalination process with consideration of feed stream preheating is employed in the RO subsystem. The feed wastewater stream is circulated by a low-pressure intake pump (IP) to the suction of a pretreatment unit for impurity removal and chemicals injection (Ghobeity and Mitsos, 2010). The pretreated stream is preheated by exchanging heat with process streams via PH-1, and then is split into two branches at point S. To be in line with the actual wastewater treatment process (Huang et al., 2019), the upper branch is pressurized by a mid-pressure pump (MPP) to reach the target pressure, while the lower one passes through a PX to recover the pressure energy from the retentate of the last stage RO block. The spiral-wound FILMTEC BW30-400 and SW30-400 @elements (Solutions, 2010) specifically designed for the desalination of brackish water and seawater are employed for the first- and second-stage RO, respectively. The aforementioned two branches mix at point M-1 and then enter the first stage RO block. The resulting retentate is further introduced to the next stage RO block by a high-pressure feed pump (HPP) for enhancing water recovery. Finally, the resulting permeate products with desired quality specification leaving these two RO blocks mix at point M-2 as the product of this integrated system.

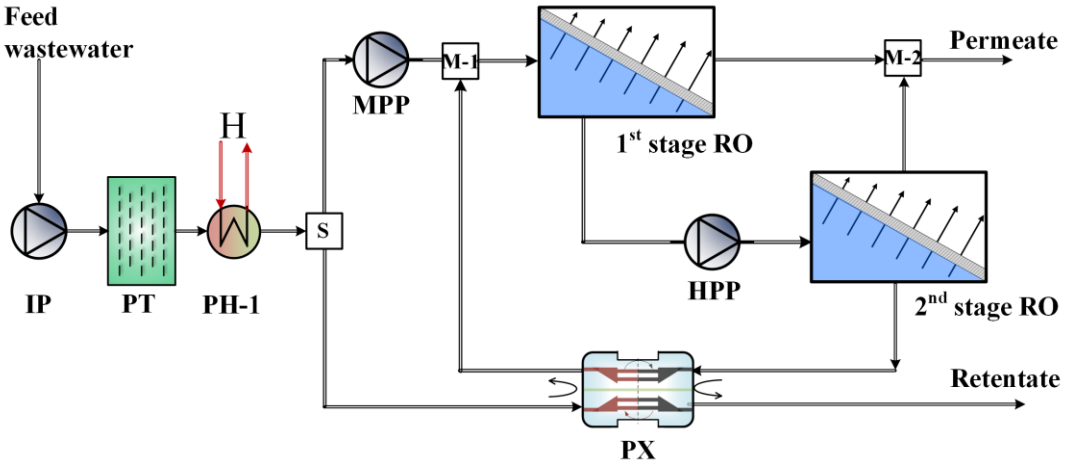

Fig. 4. Schematic diagram of the RO subsystem

The separation performance of RO membranes is mainly determined by the difference between solute and permeate permeability according to the solution diffusion model (Wang et al., 2014). For each stage of RO, the permeate flux across a membrane element is the product of the membrane permeability A_i and the net driving pressure P_i^{net}, as given by

$$J_i^P = A_i P_i^{net} = A_i(\Delta P_i^F - \overline{\Delta\Pi}_i - \frac{\Delta P_i^d}{2}),\ i \in \{1,2\} \tag{12}$$

where ΔP_i^F is the transmembrane pressure of feed stream, $\overline{\Delta\Pi_i}$ is the actual osmotic pressure difference $\Delta P_i^d/2$ is the average pressure drop between retentate and feed streams. Note that, the membrane permeability A_i should be corrected as:

$$A_i = A_{ref} \times FF \times TCF,\ \ i \in \{1,2\} \tag{13}$$

where A_{ref} is the water permeability at the reference temperature; FF and TCF are the membrane fouling factor and temperature correction factor, respectively(Ghobeity and Mitsos, 2010; Huang et al., 2019). The permeate flow rate will increase as the feed stream temperature increase (T_{SW}^{out}), the TCF can evaluate the influence aforementioned via an Arrhenius-like correlation as given by

$$TCF_i = \exp\left[\frac{Ea_i}{R}\times\left(\frac{1}{298}-\frac{1}{T_j^{out}}\right)\right],\ i\in\{1,2\};\ j\in\{SW\} \tag{14}$$

In Eq. (19), R is the ideal gas constant, Ea_i is the activation energy given by:

$$Ea_i = \begin{cases} 22000\ \text{J/mol}, & \mathrm{T}_j^{out} \le 25\ ^{\circ}\mathrm{C} \\ 25000\ \text{J/mol}, & \mathrm{T}_j^{out} > 25\ ^{\circ}\mathrm{C} \end{cases},\ i\in\{1,2\};\ j\in\{SW\} \tag{15}$$

As most of the NLP solvers require the continuous derivatives for constraints, the impulse activation energy can be smoothed by the following function

$$Ea_i = 22000 + \frac{3000}{1+e^{-\varphi(\mathrm{T}_j^{out}+25)}},\ i\in\{1,2\};\ j\in\{SW\} \tag{16}$$

where φ is a big constant typically between 10^4 and 10^6.

For each stage of RO, $\overline{\Delta\Pi_i}$ can be expressed as the product of the feed stream (Π_i^F), concentration polarization factor (CPF_i), and the concentration ratios of the feed and retentate streams (C_i^F and C_i^R) as given by Eq. (17). Note that, the phenomenon of the concentration polarization will be intensified as the increase in recovery ratio per pressure vessel (RR_i). As such, CPF_i that depends on the average recovery ratio can be approximated by constraint shown in Eq. (18) (Asatekin et al., 2007). Besides, assuming that the feed stream contains only NaCl salt, Π_i^F is calculated by Van't Hoff equation in Eq. (19).

$$\overline{\Delta\Pi_i} = CPF_i \times \frac{C_i^R}{C_i^F} \times \Pi_i^F,\ i\in\{1,2\} \tag{17}$$

$$CPF_i = \exp\left(\frac{0.7\times RR_i}{N_i^{pv}}\right),\ i\in\{1,2\} \tag{18}$$

$$\Pi_i^F = \frac{2\rho R T_j^{out}}{M_{NaCl}}(C_i^R - C_i^F),\ \ i\in\{1,2\};\ j\in\{SW\} \tag{19}$$

where N_i^{pv} denotes the number of membrane elements inside a pressure vessel; M_{NaCl}, R and ρ denote the molar mass of NaCl, ideal gas constant, and mass density of the

stream, respectively.

The salt concentrations of the permeate and retentate streams can connect with the feed concentrations by using the following constraints

$$C_i^P = (1-sr)C_i^F, \ i \in \{1,2\} \tag{20}$$

$$C_i^R = \frac{sr \times C_i^F}{1-RR_i}, \ i \in \{1,2\} \tag{21}$$

where *sr* is the salt reject factor of the membrane, which indicates the ratio of salt flux in the feed stream not across the membrane element.

The total flow rate of permeate of the system is calculated by:

$$Q_p = S^e N^e \sum_i J_i^P, \ i \in \{1,2\} \tag{22}$$

where N^e is the number of membrane elements inside an RO block and S_i^e is the active surface area for a membrane element. Once the mass balance is completed, the energy balance of the RO subsystem can be further determined, as detailed in Eqs. (S34)~(S39) in SI.

The total annualized cost of the RO subsystem (TAC_{RO}) is made up of a total of the operating cost (OC_{RO}) and the annualized capital cost ($AF \times CC_{RO}$) as given in Eq. (28). For brevity, the detailed calculations of OC_{RO} and CC_{RO} are detailed in Eqs. (S40)~(S51) in SI.

$$TAC_{RO} = OC_{RO} + AF \times CC_{RO} \tag{23}$$

4.1.4 Correlated scenarios generation

This study focuses on the generation of stochastic scenarios to properly describe the seasonal uncertainty associated with the wastewater data (salinity, flow rate, and

temperature of feed wastewater). It should be noted that some uncertain parameters (i.e., salinity and flow rate) normally have an asymmetric relationship that inevitably affects the sampling points in the space of interest (Huang et al., 2019). Sampling the space that does not appear in the real world would lead to a waste of computing resources. For addressing this issue, this study leverages the historical data provided by plant engineers and starts with an uncertainty characterization that assumes that all uncertain parameters can follow multivariate Gaussian correlated distribution, as shown in Fig.2. In this way, the uncertain parameters are mathematically modelled as a finite set of correlated scenarios with known probabilities of occurrence, and their corresponding random values restricted by the distribution boundaries are generated via the Monte Carlo sampling technique (Shastri and Diwekar, 2011). It should also be noted that the same probability of occurrence is presumed for all correlated scenarios, and each correlated scenario corresponds to a single point in the multivariate probability distribution.

In practice, the correlated scenarios can be generated from the multivariate Gaussian correlated distribution via a pseudorandom number generator implemented in MATLAB toolbox (i.e. *mvnrnd* function) based on the Mersenne algorithm (Matsumoto and Nishimura, 1998). The probability density function for correlated random parameter sets ($\boldsymbol{X}1,\ldots,\boldsymbol{X}d$) with sample size n is given by:

$$f_X(x) = \frac{1}{\sqrt{(2\pi)^n \det(\Sigma)}} \exp[-\frac{1}{2}(X-\mu)^T \Sigma^{-1}(X-\mu)] \tag{24}$$

where μ_i and det(Σ) are the mean value of each parameter set and the corresponding determinant of covariance matrix $d\boldsymbol{X}d$. The diagonal elements of Σ containing the

variances for each parameter (σ_i^2) form a symmetric positive definite matrix. The off-diagonal elements that describe the implying correlation between uncertain parameters, as given by

$$\sigma_{ij} = \rho_{ij}\sqrt{D(X_i)}\sqrt{D(X_j)} = \rho_{ij}\sigma^i\sigma^j \tag{25}$$

where ρ_{ij} and σ_{ij} denote the correlation matrix and covariance between parameters. Note that, ρ_{ij} contains the information on each pair of correlated parameters by setting all non-diagonal elements with a value between −1 and 1 (Onishi et al., 2017). Herein, a value of ρ_{ij} ranging between -1 and 0 indicates a negative correlation, while 0 and 1 indicate a positive correlation. In addition, ρ_{ij}=±1 indicates the strongest correlations and 0 indicates non-correlation. The generated correlated scenarios set is defined as $S = \{1, 2, \dots, NOS\}$. The parameter NOS indicates the number of scenarios.

4.1.5 Objective function

As shown in Fig. 2, the original optimization problem involved in this study is a deterministic NLP model where a single set of process variables is considered to obtain the minimum total annualized cost of the coupled system regardless of the cost of the heat exchangers in the HEN, which are subject to three types of constraints including the Duran-Grossmann model, ORC thermodynamic model, and RO desalination model. The generic form of the deterministic problem is given in (**P1**).

$$\begin{aligned}
&\min\ Obj = (OC_{hu}Q_{hu} + OC_{cu}Q_{cu} + TAC_{ORC} \\
&\qquad + TAC_{RO} - PGP) / (Q_p \times OT) \\
\textbf{(P1)}\qquad &s.t.\quad \text{Duran-Grossmann model Eqs.(1) ~ (8)} \\
&\qquad \text{ORC thermodynamic model Eqs.(9) ~ (16), Eqs.(S9) ~ (S28)} \\
&\qquad \text{RO desalination model Eqs.(17) ~ (34), Eqs.(S29) ~ (S46)}
\end{aligned}$$

where OC_{hu} and OC_{cu} are the operating costs related to the hot utility and cold utility.

The generated correlated scenarios along with their corresponding probabilities are then used as input data for solving the stochastic optimization problem. In particular, the underlying effects of uncertain parameters are propagated through incorporating these scenarios into detailed techno-economic modelling of the coupled system that includes detailed mass and energy balances, techno-economic equations, and constraints for each scenario, as described in Sections 4.1.1~4.1.3. The stochastic model of the coupled system is formulated as a multi-scenario NLP model as shown in (P2), which is optimized to obtain an optimal solution by minimizing the expected value of the objective distribution. The objective function accounts for the capital investment in all equipment, as well as the expected expenses related to equipment operation and maintenance (i.e., external utilities, membrane clean and replacement, and chemical dose) for desalination.

$$\min \quad Obj^{exp} = \sum_{s \in S} prob_s \times Obj_s$$

$$= \sum_{s \in S} prob_s \times \left[\left(\begin{array}{c} OC_{hu} Q_{hu} + OC_{cu} Q_{cu} + \\ TAC_{ORC} + TAC_{RO} - PGP \end{array} \right) / (Q_p \times OT) \right]_s$$

(P2) *s.t.* Duran-Grossmann model Eqs. (1) ~ (8)

ORC thermodynamic model Eqs. (9) ~ (16), Eqs. (S9) ~ (S28)

RO desalination model Eqs. (17) ~ (34), Eqs. (S29) ~ (S46)

where Obj_s denotes the total cost of the coupled system for the same scenario, and $prob_s$ denote the probability of occurrence of a specific feeding scenario s. In this model, the capital cost belongs to the scenario-independent variable, while the operating cost is formulated by stochastic functions to capture all variability in the uncertainty space. That is, the equipment capacities (such as membrane elements and pressure vessels) should be the same for all correlated scenarios.

4.2. Flexible HEN synthesis

4.2.1 Initial HEN synthesis

In this section, the techno-economic results of the coupled system obtained from Section 4.1 are improved by accounting for more precise cost data of HEN (i.e. heat exchanger investment cost) under uncertainty. For this purpose, based on a customized stage-wise superstructure (Yee and Grossmann, 1990), the initial scenarios together with their corresponding probabilities are used as input data for addressing the HEN synthesis problem. It involves a set ST = {k|1, 2, …, NOK} that stands for the stage in the superstructure, and in principle, it allows many different possibilities for stream matching to take place at each stage, as shown in Fig. 5. The only notable exception is that no heat-exchange matches existed between the streams from ORC and RO subsystems and the hot utility at the end of the superstructure.

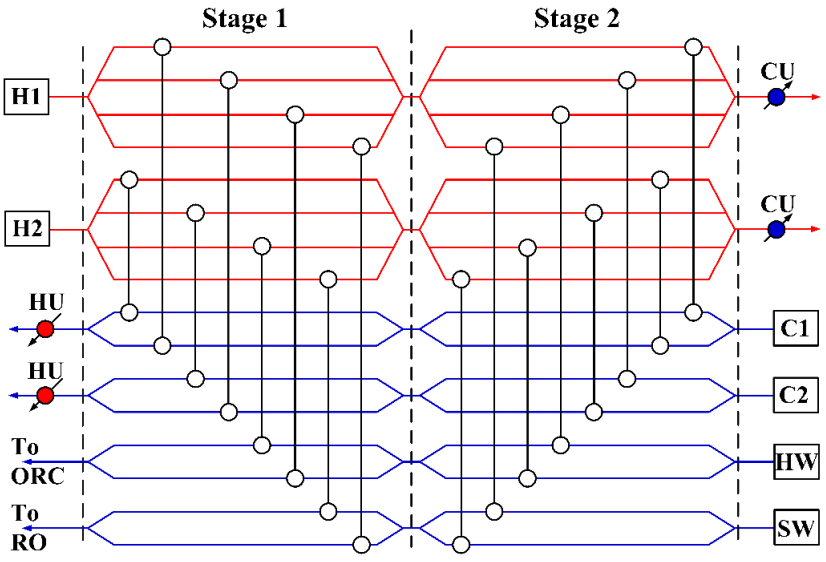

Fig. 5. Simplified stage-wise superstructure used in this work.

Once the temperature and heat capacity flow rate for each scenario are determined by solving (**P2**), the stage-wise superstructure that aims at minimizing TAC_{HEN} can be

directly applied. The mathematical model of initial HEN can be reformulated as (**P3**), in which the detailed energy balance and cost estimation are provided in Section 2.3 in SI.

$$\textbf{(P3)} \qquad \begin{aligned} &\min \quad TAC_{HEN} \quad \text{given in Eq.(S72)} \\ &s.t. \quad \text{Stage-wise superstructure Eqs.(S47) ~ (S71)} \end{aligned}$$

4.2.2 Feasibility test for multi-scenario HEN

After the optimal HEN structure for certain scenarios has been provided for a multi-scenario MINLP model, the feasibility of the HEN structure between defined conditions remains a challenge. The strategy to ensure the feasible operations of the developed HEN structure is not only in these specified scenarios but also in the whole range of the specified parameters. This is referred to as the task of keeping the outlet temperatures in the network defined by the abovementioned MINLP model at their target values during a short- or long-time horizon. Here, an LP algorithm is formulated to analyze the structural and final flexibility of the HEN (Chen and Hung, 2007). The isothermal mixing assumption remains used in the formulation to maintain the linear constraints. It guarantees the model compatible with the MINLP model, indicating that the critical conditions found with the LP model are suitable for further MINLP optimization. The LP model for the minimum temperature approach violations of a given network configuration is formulated by using the same indices and sets as used by the MINLP model.

The constraints for the LP model consist of the linear constraints as shown in Eqs. (S52)~(S73) and the following additional equations.

$$dt_{i,j,s}^{k} \le t_{i,s}^{k} - t_{j,s}^{k} + sldt_{i,j,s}^{k},\ i \in H,\ j \in C',\ k \in ST,\ s \in S,\ y_{i,j}^{k} = 1 \tag{26}$$

$$dt_{i,j,s}^{k+1} \le t_{i,s}^{k+1} - t_{j,s}^{k+1} + sldt_{i,j,s}^{k+1},\ \ i \in H,\ j \in C',\ k \in ST,\ s \in S, y_{i,j}^{k} = 1 \tag{27}$$

where $sldt_{i,j,s}^{k}$ is the slack variable for temperature approach violations related to match (i, j) at temperature location k in scenario s. Eqs. (26) and (27) are used to ensure the feasible driving forces for the existing heat exchangers by calculating the temperature differences for each temperature at each location. The fixed binary variable acquired from the result of the multi-scenario stage-wise superstructure model is used to define whether the constraint is involved or not. Additional slack variables are introduced to allow violations for feasible driving forces for existing exchangers.

The maximum allowed conductance for each exchanger $CNup_{i,j}^{k}$ is restricted by inequality constraint in Eq. (28), where the arithmetic means of temperature differences are used instead of the LMTD to avoid high nonlinearity of the model. Note that, in Eq. (29), parameters $(q_{i,j,s}^{k})_{\mathrm{MINLP}}$ and $(dt_{i,j,s}^{k})_{\mathrm{MINLP}}$ obtained from MINLP model are connected with matches ($y_{i,j,s}^{k}$=1) and scenarios with maximum exchanger areas. Therefore, the conductance of each match in the LP model is limited to be smaller than or equal to conductance related to the maximum areas of each match in the MINLP model.

$$q_{i,j,s}^{k} \le (dt_{i,j,s}^{k} + dt_{i,j,s}^{k+1}) CNup_{i,j}^{k},\ \ i \in H, j \in C', k \in ST, s \in S, y_{i,j}^{k} = 1 \tag{28}$$

$$CNup_{i,j}^{k} = \max\left[\frac{(q_{i,j,s}^{k})_{MINLP}}{(dt_{i,j,s}^{k})_{MINLP} + (dt_{i,j,s}^{k+1})_{MINLP}} \right],\ \ i \in H, j \in C', k \in ST, s \in S \tag{29}$$

The next step is to minimize the summation of the additional slack variables, i.e. temperature approach violations. The objective function is expressed as

$$\mathbb{Z} = \sum_{s \in S} \sum_{i \in H} \sum_{j \in C'} \sum_{k \in ST} (sldt_{i,j,s}^{k} + sldt_{i,j,s}^{k+1}) \tag{30}$$

The feasibility test model for multi-scenario HEN is given by

$$\textbf{(P4)}\qquad \begin{aligned} \min\ & \mathbb{Z} \text{ given in Eq. (35)} \\ s.t.\ & \text{Stage-wise superstructure Eqs. (S47) ~ (S68)} \\ & \text{LP feasibility test Eqs. (31) ~ (34)} \end{aligned}$$

The goal of this formulation is to minimize the overall violation of temperature approaches for each set of testing data. The most violating point, i.e., the testing scenario with maximum positive $\mathbb{Z}$, value over all $s \in S$, can be taken as a critical scenario for subsequent network synthesis. That is, when at least one testing scenario fails to pass the simplified LP flexibility test, the problem (**P3**) is resolved for network synthesis with the included critical scenario. The loop including the MINLP synthesis and the LP flexibility test as shown in Fig. 2 should be repeated until the resulting HEN is feasible for all test points within the specified range of parametric variations.

4.2.3 Isothermal mixing assumption removal

When stream splits take place (i.e. a given stream has two or more exchangers at a given stage), an additional NLP model is developed for removing the isothermal mixing assumption by explicitly optimizing the outlet variables at the heat exchangers with splitting. For this purpose, the NLP improvement model of HEN can be formulated as (P5), in which the mass and energy balances and the logical constraints are provided in Section 2.4 in SI.

$$\textbf{(P5)}\qquad \begin{aligned} \min\ & TAC_{HEN} \text{ given in Eq.(S85)} \\ s.t.\ & \text{Stage-wise superstructure Eqs.(S47) ~ (S62) , (S67) ~ (S71)} \\ & \text{Isothermal mixing assumption removal Eqs.(S73) ~ (S84)} \end{aligned}$$

Note that, the results of Section 4.1 provide the initial input for HEN synthesis that only accounts for the utility cost, while this section provides a rigorous cost calculation of HEN including utility cost, installation and area costs of the heat exchangers. As a

result, the utility cost derived in (P2) should be subtracted from the cost calculation to avoid the double-counting issue, and the minimal expected desalination cost per unit permeate (DCP^{exp}, $\$\cdot m^{-3}$) is given by:

$$\begin{aligned}(DCP^{exp})_{\min} &= \left[\sum_{s\in S} prob_s \times \left(\frac{TAC_{sys}}{Q_p \times OT}\right)_s\right]_{\min} \\ &= \left[\sum_{s\in S} prob_s \times \left(\frac{TAC_{ORC} + TAC_{RO} + TAC_{HEN} - PGP}{Q_p \times OT}\right)_s\right]_{\min} \\ &= (Obj^{exp})_{\min} + (TAC_{HEN})_{\min} \times \sum_{s\in S} \frac{prob_s}{(Q_p \times OT)_s} - \sum_{s\in S} prob_s \times \left(\frac{OC_{hu}Q_{hu} + OC_{cu}Q_{cu}}{Q_p \times OT}\right)_s\end{aligned} \tag{31}$$

where the TAC_{sys} is the total annualized cost of the RO-ORC-HI system.

5. Illustrative Example

The developed coupled system and solution strategy are applied to an industrial example. The background process comes from a styrene plant of PetroChina Lanzhou Petrochemical Company, which consists of five cold and five hot process streams. The properties of these background process streams are listed in Table 1. Besides, the major assumptions and parameters used for the modelling and optimization of the illustrative example are listed in Table S-1 in SI.

Table 1. The property data of background process streams

Stream	T_{in} /°C	T_{out} /°C	FCp/kW °C^{-1}
C1	192	197	950
C2	32	197	10
C3	17	132	10
C4	32	117	10
C5	192	227	20
H1	287	57	10
H2	287	57	10
H3	167	162	500
H4	97	62	30
H5	247	217	40

The statistic of daily average dry-bulb temperature during 2016~2018 retrieved from the National Oceanic and Atmospheric Administration (NOAA) database is used to construct the seasonal probability distribution functions and to estimate the statistical distribution parameters. In the correlated scenarios generation, it is assumed that the standard deviations are 5% and 10% of the nominal flow rate and salinity listed in Table 2, respectively, according to the record of plant data. Besides, the flow rate and the salinity of wastewater are negatively correlated with ρ_{ij}=-0.5, while the flow rate and the inlet temperature have a positive correlation with ρ_{ij}=0.5. In order to emphasize the importance of the stochastic method, a deterministic optimization model is also developed based on the nominal conditions (a single scenario) in each season as listed in Table 2. It should be highlighted that the deterministic model can be easily solved by using the strategy stated in Section 3. In particular, the solution of (P1) is regarded as the input of the HEN synthesis model by sequentially solving (P3) and (P5) (if needed) for a more accurate cost calculation of HEN.

Table 2. The nominal values of uncertain parameters for each season used in deterministic model.

Season	T/ ^{o}C	Flow rate/ ($m^3 \cdot h^{-1}$)	Salinity/ ppm
Spring	5.91	390	4100
Summer	20.74	420	3800
Autumn	15.99	400	4000
Winter	-2.23	380	4200

For each season, the uncertainty on feed data can be mathematically modeled using 20 distinct scenarios, resulting in a total number of 80 scenarios (see Table S-2 in SI) that are investigated in the stochastic model. The models (P1)~(P5) are formulated

using GAMS 24.4 modelling environment and solved on a workstation with an Intel Xeon E5 at 2000 MHz with 128 GB memory. GAMS/CONOPT 3.0 (Drud, 1994) is used to solve the NLP problems, GAMS /DICOPT (Kocis and Grossmann, 1989) is used for the MINLP problems (Ipopth and the Gurobi 6.0 are NLP and MILP sub-solvers in the DICOPT, respectively), GAMS/ Gurobi 6.0 is employed for solving the LP problems. The final reports show that the optimal solutions for the NLP and LP problems can be obtained within 0.03~10 CPUs, and for the MINLP problem within 120~420 min. More detailed iteration processes for HEN synthesis can be found in Section 5 in SI.

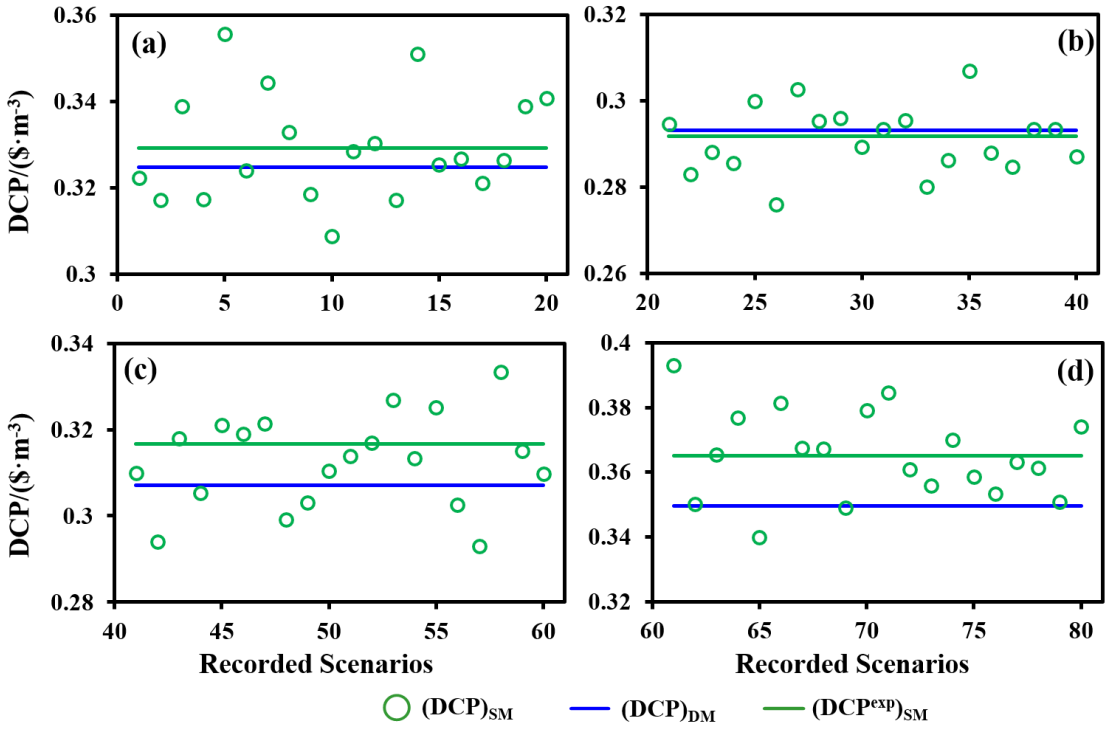

Fig. 6. The desalination cost distribution of the coupled system in (a) spring, (b) summer, (c) autumn, and (d) winter. The subscripts DM and SM denote the deterministic and stochastic methods.

Fig. 6 presents the scatter plots of the optimal desalination cost obtained from both the stochastic and deterministic methods. For a better understanding of the impact of uncertainty on system's performance, the green circles denoting the stochastic solutions are grouped into four distinct cases according to the corresponding seasons. The green line across the circles denotes the average performance of the stochastic solutions in terms of the expected value of desalination costs, which is \$0.329 m^{-3} for the spring case, \$0.292 m^{-3} for the summer case, \$0.317 m^{-3} for the autumn case, and \$0.365 m^{-3} for the winter case. Fig. 6 also presents the optimal desalination costs based on perfect information (no uncertainty) by solving the deterministic model for the four cases. As denoted by blue lines, the desalination costs are \$0.325 m^{-3}, \$0.293 m^{-3}, \$0.307 m^{-3},

and \$0.350 m^{-3}, respectively. This increment of the desalination costs indicates that the incorporation of wastewater variability in process design and optimization can lead to additional costs. Besides, it is seen that the desalination costs in winter and spring are relatively higher than those in summer and autumn for both deterministic and stochastic solutions. This reflects that the increase in salinity of wastewater in cold seasons contributes more portion to the desalination cost, compared with the increase in flow rate in hot seasons.

The feasibility of synthesized HEN grids should be examined in the model (**P4**) by using a set of testing scenarios to meet the heat transfer requirement. For presenting a clearer result of the examination, a binary parameter $\Theta(s)$ defined in Eq. (32) is used as an index according to the optimal value of the summation of the additional slack variables in the solution of (**P4**). For example, $\Theta(s)=0$ represents that the HEN structure is suitable for the testing scenario (s).

$$\Theta(s)=\begin{cases}0, & \mathbb{Z}=0\\ 1, & \mathbb{Z}>0\end{cases},\quad s\in S \tag{32}$$

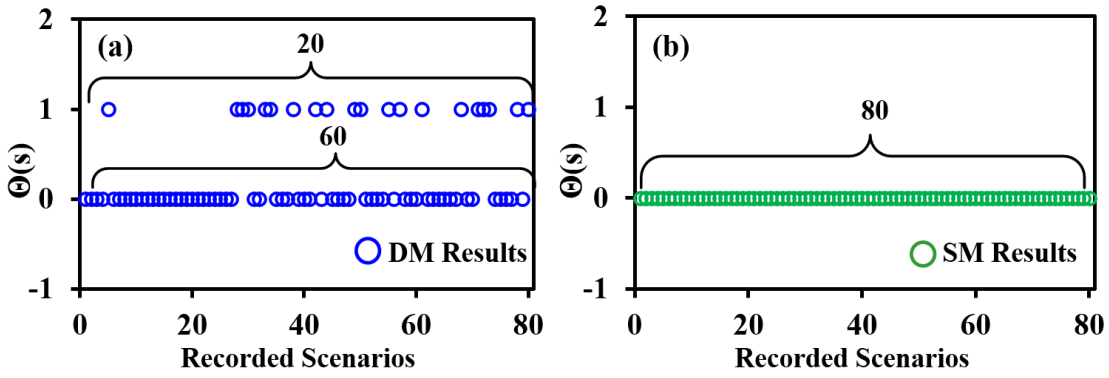

Fig. 7. The feasibility test results of the HEN structure. (a) Deterministic solution and (b) stochastic solution.

All 80 scenarios listed in Table S-1 in SI are regarded as the testing scenarios and the resulting $\Theta(s)$ are shown in Fig. 7. It can be found that for the deterministic method, only 60 testing scenarios, accounting for 75 % of the total satisfy the heat transfer requirement ($\Theta(s)=0$). By contrast, the satisfactory scenarios can remarkably increase to 80 for the stochastic method. From the comparison, we can conclude that as the uncertainty on wastewater is considered in the HEN design of the coupled system, the deterministic solution based on the nominal conditions is far from flexible in comparison with the stochastic one despite its relatively low desalination cost.

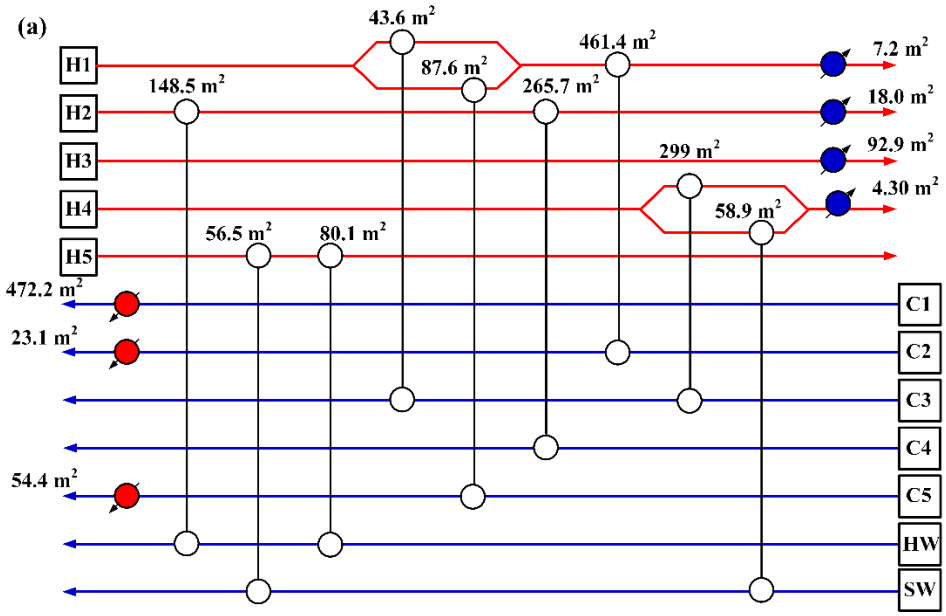

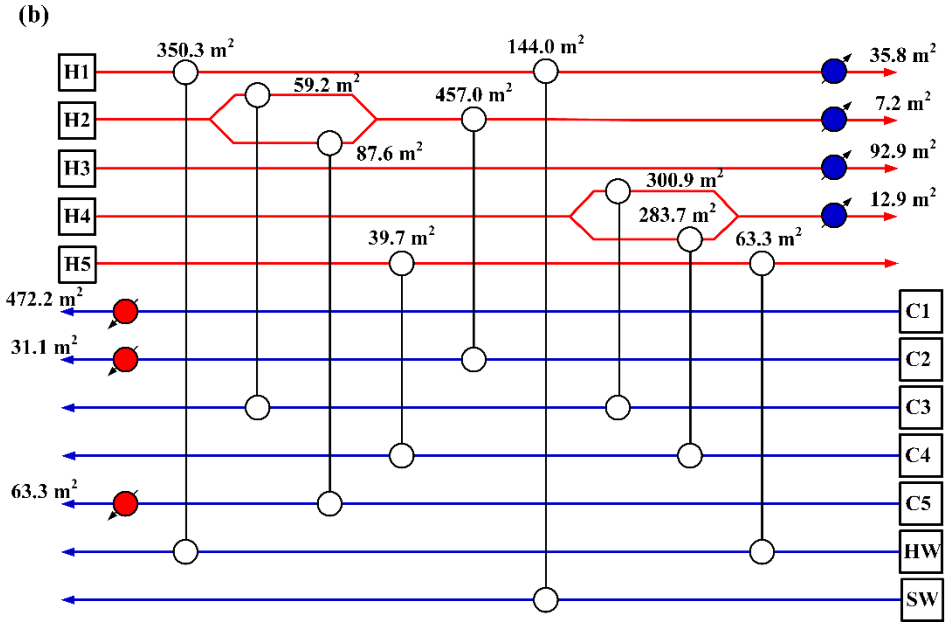

Fig. 8. The optimal HEN grids obtained from the (a) deterministic solution and (b) stochastic solution.

Fig. 8 presents the optimal solutions of the HEN grids obtained from both methods after removing the isothermal mixing assumption in model (**P5**). As shown in this figure, both solutions yield different HEN structures especially for the process-process heat exchangers, although the numbers and areas of the heat exchangers are closed to each other. Note that, the hot utilities for both solutions have reached their upper bounds and thus the resulting numbers and areas of the heaters are completely the same as shown on the left side of Fig. 8. The annualized area cost of the HEN grid for the stochastic solution is \$0.067MM, which is only 1.64% higher than that of the deterministic one. By combining the results from Figs. 7 and 8, it can be found that the slight increase in the economic cost of the heat exchangers and the rearrangement of the HEN structure can bring significant benefits for the flexibility of the HEN structure. Therefore, the following sections are merely focused on the stochastic solution.

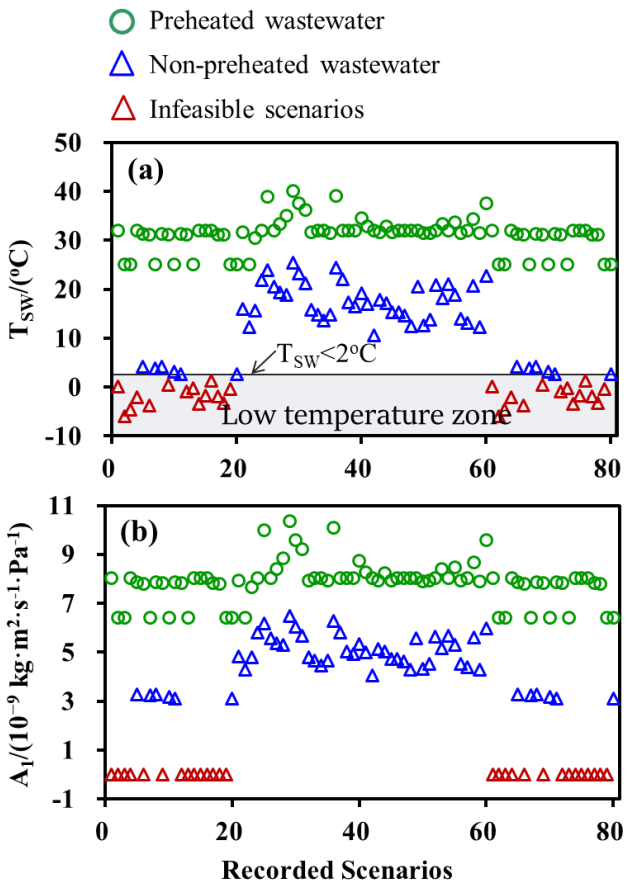

Fig. 9. The comparisons of the feed wastewater *w/wo* preheating operation for the stochastic solution. (a) Inlet temperature and (b) Membrane permeability.

Fig. 9 reveals the underlying effects of preheating and non-preheating operations for the wastewater stream in terms of inlet temperature and membrane permeability. As shown in Fig. 9(a), the optimal temperatures of preheated wastewater denoted by green circles are 1.04 ~16.97 % higher than that of the non-preheated wastewater denoted by triangles depending on the specific scenarios. According to the industrial experience of plant engineers, it is suggested that the requirement for the feed solution temperature is between 2°C and 42°C. From Fig. 9(a), it is seen that for the non-preheating operation, a total of 28 feeding scenarios denoted by red triangles that fall in the low-temperature zone are not satisfying this requirement, while the unsatisfactory scenarios sharply drop

to zero for the preheating operation. The RO membrane permeability is directly related to the temperature of the feed solution according to Eqs. (14)~(16). This leads to the same number of unsatisfactory scenarios with infeasible membrane permeability, as shown in Fig. 9(b). Excluding these infeasible scenarios, the RO membrane permeability can still increase by 10.63 ~ 158.64 % compared with the non-preheating operation.

Although an increased temperature of the feed solution intensifies the membrane permeability and improves the permeate productivity, the benefit is significant only as the temperature variation covers a limited range. As reflected by the green circles in Fig. 9(a), there are almost none of the scenarios reaching the upper bound of the specified temperature range. This is because a higher preheating temperature for feed wastewater not only reduces the energy allocated to ORC for power generation, but also in turn lowers the net driving pressure of the RO membrane to a certain degree. This highlights the importance of providing external energy for addressing uncertainty on wastewater by properly adjusting its inlet temperature, especially in cold seasons.

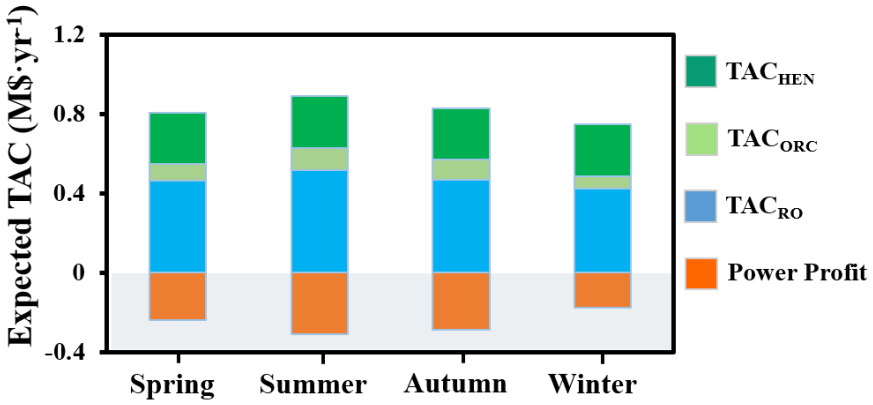

Fig. 10. Breakdown of expected TAC of the coupled system for each season.

Fig. 10 shows the detailed cost breakdowns of the expected total annualized cost of the coupled system for the stochastic solution. From the positive axis of this figure, it is clear that TAC_{HEN} and TAC_{RO} account for the major shares of the total for both methods. The remaining minor contribution (only 7.06%) comes from TAC_{ORC}. Note that, the sum of TAC_{HEN}, TAC_{RO}, and TAC_{ORC} for all seasons are nearly the same. A major reason for this phenomenon is that the annual capital cost of each subsystem based on the scenarios of one season is equal to that based on the other one for the same solution. In this case, thus the profit of power generation becomes a key contributor to determine the final TAC of the coupled system. As shown, for both methods the annualized power profit drops from a hot season to a cold season, and the resulting ranking is as follows: summer>autumn>spring>winter. The corresponding profit values are \$0.311MM, \$0.286 MM, \$0.238MM, and \$0.178MM, respectively.

In Fig. 10, it is interesting that for both methods the TAC_{ORC} has a similar tendency to the power profit. In summer and autumn, on average the TAC_{ORC} is 21.3~74.43% higher than that of the spring and winter. However, the TAC_{RO} has an opposite tendency, and the values based on the spring and winter are slightly 0.99~22.24% higher than those based on the summer and autumn. This can be attributed to the fact that there is a trade-off between ORC and RO for obtaining available resources of waste heat from the background process. More specifically, the amount of waste heat allocated to preheat wastewater stream is very sensitive to the inlet temperature depending on the exact realization of uncertainty, which can be reflected by the temperature profiles shown in Fig. 9. Consequently, in cold seasons like spring and winter, RO is inclined

to absorb more waste heat for preheating feed wastewater, which can effectively improve the productivity of permeate. On the contrary, in summer and autumn, a greater portion of available waste heat is supplied for increasing the power profit in the ORC subsystem. This phenomenon reflects that the uncertainty of feed wastewater varying with seasons results in the competition and cooperation between the ORC and RO subsystems.

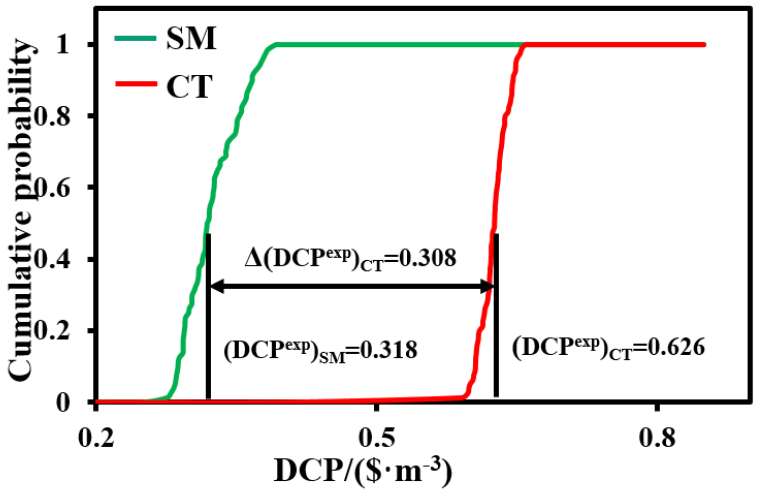

Fig. 11. Cumulative probability curves for the desalination costs of current work against conventional technology. The subscripts SM and CT denote the solutions based on the current work and the conventional BWRO technology.

In Fig. 11, the results of green circles in Fig. 6 in each season are rearranged to better present the corresponding possibility distribution, as denoted by the green curve. Besides, the desalination cost of brackish water RO (BWRO) based on conventional stand-alone plants, which in fact vary with the capacities of the plants regarding flow rate of permeate according to the following correlation derived from Bhojwani et al., (2019).

$$(\mathrm{DCP})_{\mathrm{CT}} = \begin{cases} -4.2\times10^{-4}Q_p + 0.778, & Q_p \in (157, 788) \\ -8.5\times10^{-5}Q_p + 0.514, & Q_p \in (788, 1577) \\ -1.3\times10^{-5}Q_p + 0.4, & Q_p \in (1577, 7558) \end{cases} \quad (33)$$

Using the aforementioned correlation, we estimate the stochastic desalination cost of the conventional BWRO plants by applying the optimal flow rate of permeate in each scenario. The corresponding cumulative probability is represented by the red curve in Fig. 11. As shown, the solutions of desalination cost obtained from the conventional BWRO technology and the stochastic model are concentrated at the ranges of \$0.59 ~0.66 m^{-3} and \$0.28~0.39 m^{-3}. Accordingly, the average economic performance in terms of the expected desalination cost has almost halved from \$0.626m^{-3} to \$0.308m^{-3}. The widening gap between the two solutions implies that the proposed system and the solution strategy can bring huge benefits to the techno-economic performance of the desalination system compared with the conventional technology.

6. Conclusions

This study presented a new industrial waste heat-powered wastewater desalination system that integrated RO and ORC into a background process with HI to minimize the expected desalination cost under seasonal uncertainty on the feed wastewater (salinity, flow rate, and temperature). It provided more opportunities that not only can efficiently recover the waste heat from the background process for sustainable desalination, but intensified the RO membrane permeability by properly preheating the feed wastewater. In order to attain an optimal design, the problem was decomposed into five sub-problems and solved sequentially by a two-step solution strategy. In the first step, the seasonal uncertainty on the wastewater was characterized and quantitated by generating

a finite size of scenarios via a stochastic generation method. The uncertainty realization was then embedded in a Pinch-based Duran-Grossman model for minimizing the expected desalination cost ignoring a detailed HEN topology. In the second step, based on a customized stage-wise superstructure, a flexible HEN synthesis model that minimized the total annualized cost of HEN of the coupled system was proposed and solved by sequential flexibility test and isothermal mixing assumption removal. In this way, the optimal design of the coupled system with flexible HEN was obtained.

An illustrative example was presented to evaluate the applicability of the proposed solution strategy through its comparison with a deterministic method. The optimization results indicated that the desalination costs obtained from the stochastic solution ranged from \$0.28 m^{-3} to \$0.39m^{-3} depending on the exact realization of uncertainty, which were slightly higher than that of the deterministic solution by 0.85~2.71% in most seasons. Nevertheless, the economic cost brought significant benefits to strengthen the system's flexibility and to reduce the feasibility risks of the HEN during plant operation. Besides, the non-preheating operation resulted in a total of 20 infeasible scenarios accounting for 25% of the total that unsatisfied the temperature requirement. As for the preheating operation, the unsatisfactory scenarios dropped to zero and the membrane permeability raised by 1.04~16.97 % compared with the non-preheating operation. Finally, the desalination cost of the stochastic solution of the coupled system was compared with the conventional stand-alone BWRO plants. The comparison results showed that the expected desalination cost had almost halved from \$0.626 m^{-3} for the BWRO to \$0.308 m^{-3} for the stochastic solution, indicating that the proposed RO-ORC-

HI system and the solution strategy can substantially improve the techno-economic performance of the desalination system.

Declaration of competing interest

The authors declare that they have no known competing financial interests or personal relationships that could have appeared to influence the work reported in this paper.

Acknowledgments

Financial supports from the National Natural Science Foundation of China (51776228) and Fundamental Research Funds for the Central Universities (20lgpy01) are gratefully acknowledged.

Reference

[1] Abdelhady, F., Bamufleh, H., El-Halwagi, M.M., Ponce-Ortega, J.M., 2015. Optimal design and integration of solar thermal collection, storage, and dispatch with process cogeneration systems. Chemical Engineering Science 136, 158-167.

[2] Asatekin, A., Kang, S., Elimelech, M., Mayes, A.M., 2007. Anti-fouling ultrafiltration membranes containing polyacrylonitrile-graft-poly(ethylene oxide) comb copolymer additives. Journal of Membrane Science 298(1-2), 136-146.

[3] Balakrishna, S., Biegler, L.T., 1992. Targeting strategies for the synthesis and energy integration of nonisothermal reactor networks. Industrial & Engineering Chemistry Research 31(9), 2152-2164.

[4] Bhojwani, S., Topolski, K., Mukherjee, R., Sengupta, D., El-Halwagi, M.M., 2019. Technology review and data analysis for cost assessment of water treatment systems. Science of the Total Environment 651, 2749-2761.

[5] Cao, Z., Deng, J., Ye, F., Garris Jr, C.A., 2018. Analysis of a hybrid Thermal Vapor Compression and Reverse Osmosis desalination system at variable design conditions. Desalination 438, 54-62.

[6] Chen, C.L., Chang, F.Y., Chao, T.H., Chen, H.C., Lee, J.Y., 2014. Heat-Exchanger Network Synthesis Involving Organic Rankine Cycle for Waste Heat Recovery. Industrial & Engineering Chemistry Research 53(44), 16924-16936.

[7] Cignitti, S., Andreasen, J.G., Haglind, F., Woodley, J.M., Abildskov, J., 2017. Integrated working fluid-thermodynamic cycle design of organic Rankine cycle power systems for waste heat recovery. Applied Energy 203, 442-453.

[8] Delgado-Torres, A.M., García-Rodríguez, L., 2010. Preliminary design of seawater and brackish water reverse osmosis desalination systems driven by low-temperature solar organic Rankine cycles (ORC). Energy Conversion and

Management 51(12), 2913-2920.

[9] Desai, N.B., Bandyopadhyay, S., 2009. Process integration of organic Rankine cycle. Energy 34(10), 1674-1686.

[10] Dong, X., Liao, Z., Sun, J., Huang, Z., Jiang, B., Wang, J., Yang, Y., 2020. Simultaneous optimization for organic rankine cycle design and heat integration. Industrial & Engineering Chemistry Research 59(46), 20455-20471.

[11] Drud, A.S., 1994. CONOPT—a large-scale GRG code. ORSA Journal on computing 6(2), 207-216.

[12] Duran, M.A., Grossmann, I.E., 1986. Simultaneous optimization and heat integration of chemical processes. AIChE Journal 32(1), 123-138.

[13] Geng, D., Du, Y., Yang, R., 2016. Performance analysis of an organic Rankine cycle for a reverse osmosis desalination system using zeotropic mixtures. Desalination 381, 38-46.

[14] Elsido, C., Cremonesi, A., Martelli, E., 2021a. A novel sequential synthesis algorithm for the integrated optimization of Rankine cycles and heat exchanger networks, Applied Thermal Engineering 192, 116594,

[15] Elsido, C., Martelli, E., Grossmann, I.E. 2021b. Multiperiod optimization of heat exchanger networks with integrated thermodynamic cycles and thermal storages. Computers & Chemical Engineering 149, 107293.

[16] Ghobeity, A., Mitsos, A., 2010. Optimal time-dependent operation of seawater reverse osmosis. Desalination 263(1-3), 76-88.

[17] Goh, P.S., Kang, H.S., Ismail, A.F., Hilal, N. 2021. The hybridization of thermally-driven desalination processes: the state-of-the-art and opportunities. Desalination 506, 115002.

[18] Hafizan, A.M., Wan Alwi, S.R., Manan, Z.A., Klemeš, J.J., Abd Hamid, M.K., 2020. Design of optimal heat exchanger network with fluctuation probability using break-even analysis. Energy 212, 118583.

[19] Huang, L., Wang, D., He, C., Pan, M., Zhang, B., Chen, Q., Ren, J., 2019. Industrial wastewater desalination under uncertainty in coal-chemical eco-industrial parks. Resources, Conservation and Recycling 145, 370-378.

[20] Jin, X., Jawor, A., Kim, S., Hoek, E.M.V., 2009. Effects of feed water temperature on separation performance and organic fouling of brackish water RO membranes. Desalination 239(1-3), 346-359.

[21] Janajreh, I., Hasania, A., Fath, H., 2013. Numerical simulation of vapor flow and pressure drop across the demister of MSF desalination plant. Energy Conversion and Management 65, 793-800.

[22] Kang, L., Liu Y., 2019. Synthesis of flexible heat exchanger networks:a review. Chinese Journal of Chemical Engineering 27(7), 1485-1497.

[23] Kocis, G.R., Grossmann, I.E., 1989. Computational experience with DICOPT solving MINLP problems in process systems engineering. Computers & Chemical Engineering 13(3), 307-315.

[24] Li, M., 2015. Analysis and optimization of pressure retarded osmosis for power generation. AIChE Journal 61(4), 1233-1241.

[25] Mahmoudi, A., Fazli, M., Morad, M. R., 2018. A recent review of waste heat recovery by organic rankine cycle. Applied Thermal Engineering 143, 660-675.

[26] Martelli, E., Elsido, C., Mian, A., Marechal, F., 2017. MINLP model and two-stage algorithm for the simultaneous synthesis of heat exchanger networks, utility systems and heat recovery cycles. Computers & Chemical Engineering 106, 663–689.

[27] Matsumoto, M., Nishimura, T., 1998. Mersenne twister: a 623-dimensionally equidistributed uniform pseudo-random number generator. ACM Transactions on Modeling and Computer Simulation (TOMACS) 8(1), 3–30.

[28] Mohammed, R.H., Ibrahim, M.M., Abu-Heiba, A., 2021. Exergoeconomic and

multi-objective optimization analyses of an organic Rankine cycle integrated with multi-effect desalination for electricity, cooling, heating power, and freshwater production. Energy Conversion and Management 231, 113826.

[29] Onishi, V.C., Ruiz-Femenia, R., Salcedo-Díaz, R., Carrero-Parreño, A., Reyes-Labarta, J.A., Fraga, E.S., Caballero, J.A., 2017. Process optimization for zero-liquid discharge desalination of shale gas flowback water under uncertainty. Journal of Cleaner Production 164, 1219-1238.

[30] Pan, S.Y., Haddad, A.Z., Kumar, A., Wang, S.W., 2020. Brackish water desalination using reverse osmosis and capacitive deionization at the water-energy nexus. Water Research 183, 116064.

[31] Ratnam, R., Patwardhan, V.S., 1991. Sensitivity analysis for heat exchanger networks. Chemical Engineering Science 46(2), 451-458.

[32] Schilling, J., Entrup, M., Hopp, M., Gross, J., Bardow, A., 2021. Towards optimal mixtures of working fluids: integrated design of processes and mixtures for Organic Rankine Cycles. Renewable and Sustainable Energy Reviews 135, 110179.

[33] Shaaban, S., Yahya, H., 2017. Detailed analysis of reverse osmosis systems in hot climate conditions. Desalination 423, 41-51.

[34] Shastri, Y., Diwekar, U., 2011. Stochastic Modeling for Uncertainty Analysis and Multiobjective Optimization of IGCC System with Single-Stage Coal Gasification. Industrial & Engineering Chemistry Research 50(9), 4879-4892.

[35] Solutions, D.W., 2010. Filmtec™ Reverse Osmosis Membranes. Technical Manual Form, 399(609-00071), 1-180.

[36] Mansouri, M.T., Amidpour, M., Ponce-Ortega, J.M., 2019. Optimal integration of organic Rankine cycle and desalination systems with industrial processes: Energy-water-environment nexus. Applied Thermal Engineering 158, 113740.

[37] Varga, Z., Rabi, I., Farkas, C., 2012. Waste Heat Recovery with Organic Rankine Cycle in the Petroleum Industry. Chemical Engineering Transactions 29, 301-306.

[38] Wang, J., Dlamini, D.S., Mishra, A.K., Pendergast, M.T.M., Wong, M.C.Y., Mamba, B.B., Freger, V., Verliefde, A.R.D., Hoek, E.M.V., 2014. A critical review of transport through osmotic membranes. Journal of Membrane Science 454, 516-537.

[39] Wang, S., Zhu, Q., He, C., Zhang, B., Chen, Q., Pan, M., 2018. Model-based optimization and comparative analysis of open-loop and closed-loop RO-PRO desalination systems. Desalination 446, 83-93.

[40] Yee, T.F., Grossmann, I.E., 1990. Simultaneous optimization models for heat integration—II. Heat exchanger network synthesis. Computers & Chemical Engineering 14(10), 1165-1184.

[41] Yu, H., Eason, J., Biegler, L.T., Feng, X., 2017. Simultaneous heat integration and techno-economic optimization of Organic Rankine Cycle (ORC) for multiple waste heat stream recovery. Energy 119, 322-333.

[42] Zhang, T., Liu, L., Hao, J., Zhu, T., Cui, G., 2021. Correlation analysis based multi-parameter optimization of the organic Rankine cycle for medium- and high-temperature waste heat recovery. Applied Thermal Engineering 188, 116626.

[43] Zhang, X., Yin, H., Huo, Z., 2011. Flexible synthesis of heat exchanger network with particle swarm optimization algorithm, Advanced Materials Research 214, 569-572.

[44] Zhu, Q., Zhang, B., Chen, Q., Pan, M., Ren, J., He, C., 2017. Optimal synthesis of water networks for addressing high-concentration wastewater in coal-based chemical plants. ACS Sustainable Chemistry & Engineering 5(11), 10792-10805.